DOI: 10.1002/anie.201108708

Ceria Foams

Ceria Foam with Atomically Thin Single-Crystal Walls**

*Jun Xing, Hai Feng Wang, Chen Yang, Dong Wang, Hui Jun Zhao, Guan Zhong Lu, P. Hu, and Hua Gui Yang**

Porous solids are of scientific and technological interest because of a wide range of emerging applications.[1–5] Up to now, the soft or hard templating route is still the major synthetic strategy to create high-surface-area *meso*- or macroporous inorganic materials, including carbon, simple metal oxides, multiple metal oxides, metal sulfides, and metal nitrides.[6,7] For the soft template method to fabricate porous transition metal oxides in which organic structure-directing agents (SDA) are involved, the main problem is that the temperature required for the crystallization is normally high and the liquid crystals of organic SDA templating the metal oxide would decompose before the amorphous walls of metal oxides start to crystallize. Often such materials were not fully crystalline but instead composed of nanocrystals embedded in amorphous matrix to form a semicrystalline structure owing to the low treatment temperature (400–450 °C).[8] The hard templating method is an alternative approach developed to obtain high crystallinity without structural collapse.[9] Moreover, even if rigid templates such as mesoporous carbon or silica materials are applied, this strategy suffers some disadvantages, such as tedious synthesis processes, the use of undesirable reagents (such as HF), and hardly any mesostructure produced with ultrathin walls. Thus, it is essential to develop new facile synthetic strategies to fabricate non-siliceous metal oxides in porous form with highly crystalline walls.

Ceria (CeO_2) is one of the most studied functional metal oxides, and it is extensively used in clean energy and environmental protection areas, such as solar-driven thermochemical CO_2 reduction, solid oxide fuel cells, solar cells, CO oxidation, and biomass reforming.[10–16] For all of these applications, the efficacies largely depend on the specific surface area and degree of crystallinity of CeO_2. The grain boundaries of primary CeO_2 building blocks also need to be minimized to facilitate the electron transfer for redox or photovoltaic processes. Thus, fabricating CeO_2 porous architectures with high surface area and long-range single crystalline walls is highly desired to enhance the performance of these catalytic or photovoltaic applications. However, owing to the cubic crystal structure, which lacks an intrinsic driving force for continuous anisotropic crystal growth, the synthesis of porous ceria with ultrathin single-crystalline walls has attained very limited success and still remains a major challenge.

Herein, using scheelite-type $CeGeO_4$ as starting material, we report a new facile thermal decomposition process under an ammonia (NH_3) atmosphere to fabricate three-dimensional (3D) CeO_2 foams with long-range atomically thin single-crystalline walls. First-principles calculations were also performed to understand the feasibility and reaction pathways of thermal decomposition of $CeGeO_4$. To our knowledge, this is the first report of a 3D foam of a metal oxide with an ultrathin (4–8 Å) single-crystalline wall.

CeO_2 foam with atomically thin single-crystalline wall was synthesized by a two-step method. First, scheelite-type $CeGeO_4$ crystals prepared by a facile hydrothermal process were used as the solid precursor. The synthetic method involves keeping cerium (III) nitride aqueous solution containing GeO_2 powder and citric acid in a Teflon-lined stainless autoclave under 200 °C for 24 h. The as-prepared $CeGeO_4$ crystals were then treated under NH_3 atmosphere at (780 ± 20) °C (see the Experimental Section in the Supporting Information for details). After heat treatment in an NH_3 atmosphere, the color of the sample changed from white to yellow-green and the volume dramatically expanded, as also illustrated in a digital camera image (Figure 1a). The crystal-phase transformation during the entire synthesis was monitored by wide-angle X-ray diffraction (XRD) (Figure 1b). The XRD pattern of the as-synthesized $CeGeO_4$ crystals matches well with the tetragonal structure of scheelite-type $CeGeO_4$ (*141/a*, $a = b = 5.043$ Å, $c = 11.174$ Å; JCPDS Card

[*] J. Xing,[+] Dr. C. Yang,[+] Prof. Dr. H. G. Yang
Key Laboratory for Ultrafine Materials of Ministry of Education, School of Materials Science and Engineering, East China University of Science and Technology
Shanghai, 200237 (China)
E-mail: hgyang@ecust.edu.cn
Prof. Dr. P. Hu
School of Chemistry and Chemical Engineering
The Queen's University of Belfast, Belfast, BT9 5AG (UK)
Dr. H. F. Wang,[+] D. Wang, Prof. G. Z. Lu
Labs for Advanced Materials, Research Institute of Industrial Catalysis, East China University of Science and Technology
Shanghai, 200237 (China)
Prof. H. J. Zhao
Centre for Clean Environment and Energy, Gold Coast Campus
Griffith University, Queensland 4222 (Australia)
[+] These authors contributed equally to this work.

[**] This work was financially supported by Scientific Research Foundation of East China University of Science and Technology (YD0142125), Pujiang Talents Programme of Science and Technology Commission of Shanghai Municipality (09J1402800), Shuguang Talents Programme of Education Commission of Shanghai Municipality (09SG27), National Natural Science Foundation of China (20973059, 91022023, 21076076), Fundamental Research Funds for the Central Universities (WJ0913001), Program for Prof. of Special Appointment (Eastern Scholar) at Shanghai Institutions of Higher Learning, and Program for New Century Excellent Talents in University (NCET-09-0347)

Supporting information for this article is available on the WWW under http://dx.doi.org/10.1002/anie.201108708.

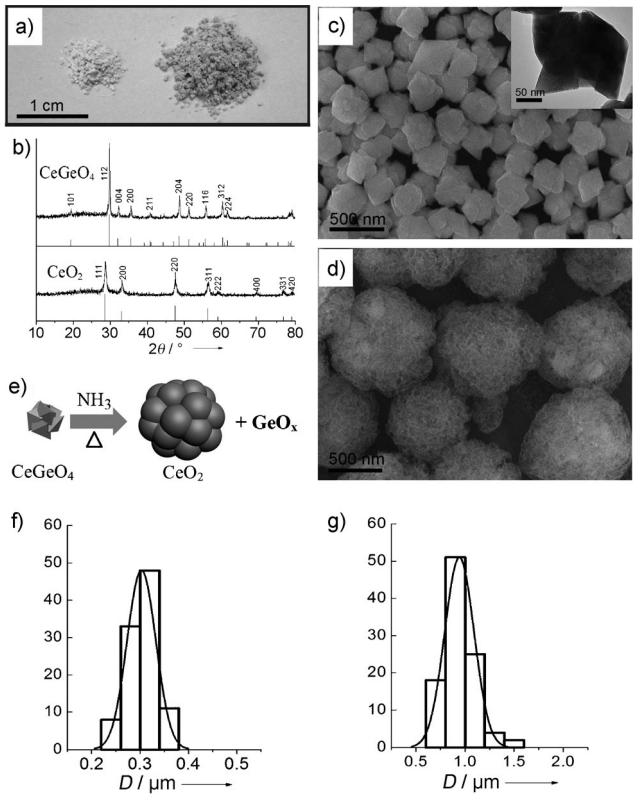

Figure 1. a) Digital camera image of the starting $CeGeO_4$ crystals (left) and the CeO_2 foam (right) generated after NH_3 treatment. b) Typical XRD patterns of the starting $CeGeO_4$ crystals and the CeO_2 foam. c) SEM image of starting $CeGeO_4$ crystals (inset: corresponding TEM image; scale bar 50 nm). d) SEM image of CeO_2 foam. e) Illustration of the conversion process from $CeGeO_4$ crystal to CeO_2 foam. f,g) Statistical analysis of size distribution of $CeGeO_4$ crystals and CeO_2 foam. Average $D = 0.303$ μm (f), 0.950 μm (g). The relative standard deviations of all statistical data (10.01% (f), 17.4% (g)) were derived from counting 100 particles for each sample.

No. 40-1182). Once $CeGeO_4$ crystals were heat-treated in an NH_3 atmosphere, all of the diffraction peaks of the sample obtained could be indexed to a pure cubic CeO_2 phase (*Fm*3*m*, $a = 5.4113$ Å; JCPDS Card No. 34-0394). Heat treatment of $CeGeO_4$ crystals in ambient atmosphere at the same temperature was also attempted, and phase conversion of $CeGeO_4$ crystal did not occur (Supporting Information, Figure S1a). The morphology and size of $CeGeO_4$ crystals did not change either (Supporting Information, Figure S1b). Thus, it can be confirmed that NH_3 may play an important role in the thermal decomposition of $CeGeO_4$ crystals to form ceria foam. Moreover, the weight of sample decreased by 19% after heat-treatment in an NH_3 atmosphere, which is attributed to $CeGeO_4$ crystal decomposition and partial germanium volatilization (37.8% of the theoretical weight ratio of GeO_2 in $CeGeO_4$). Figure 1c shows a typical scanning electron microscope (SEM) image of the synthesized $CeGeO_4$ crystals used as the solid precursor to generate CeO_2 foam. The $CeGeO_4$ particles have a sphere-like morphology with a relatively uniform size. The inset of Figure 1c is an enlarged transmission electron microscopy (TEM) image of $CeGeO_4$ crystals, and every sphere-like crystal consists of several regular octahedra. Based on the SEM observation in Figure 1d, the volume expanding observed should be mainly due to the formation of CeO_2 foam-like spheres. According to the above analysis, the formation process of CeO_2 foam can be identified (Figure 1e). To examine the volume change of the samples before and after heat treatment in NH_3, we statistically analyzed the values of the diameters D of original $CeGeO_4$ crystals and CeO_2 foams. The results are presented in Figure 1f,g: the average values of D are 0.303 μm and 0.950 μm with relative standard deviations of 10.1% and 17.4%, respectively, indicating that the diameter and the volume of CeO_2 foam are approximately 3.1 times and 30 times larger than that of original $CeGeO_4$ crystals. To explore the formation mechanism of ceria foam, the effect of nitridation temperature was also investigated. The morphology of the sample treated at NH_3 atmosphere at 700 °C was similar to that of original $CeGeO_4$ crystals (Supporting Information, Figure S2), although the crystal phase still changed into a cubic CeO_2 phase.

TEM was used to further understand the inherent structure of the as-synthesized CeO_2 foam. As shown in Figure 2a,b and Supporting Information, Figure S3, these sphere foams were formed by overlaying of many small

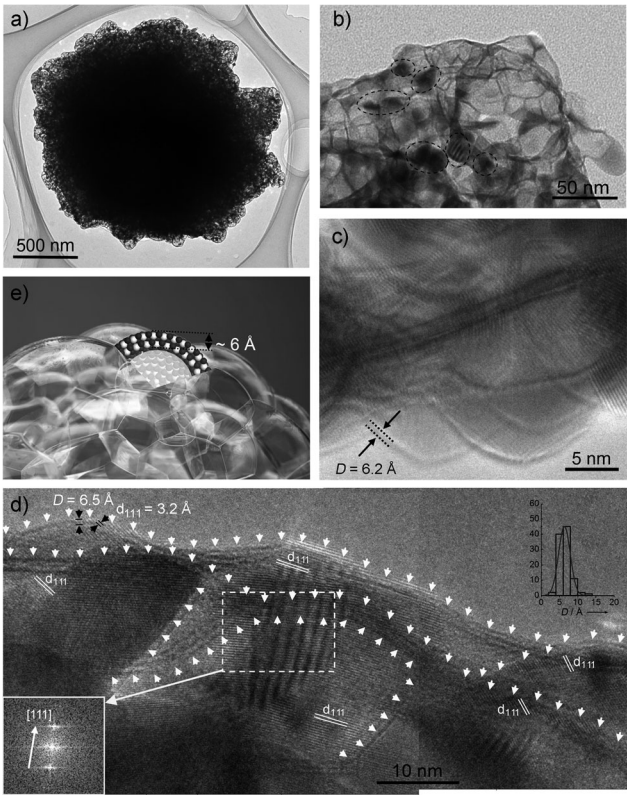

Figure 2. a,b) Typical TEM images with different magnification. c,d) Typical high-resolution TEM images. e) Digital camera photograph of soap bubble with a model of the wall of CeO_2 foam inserted. Insets in (d): FFT patterns obtained from the HRTEM image and statistical analysis of thickness distribution of walls of CeO_2 foam (average $D = 6.41$ Å, relative standard deviation (22.5%) derived from counting 50 walls and two different points of each wall were measured. The areas marked by black dotted circles in (b) indicate some small particles in the CeO_2 foam. The vertical stripes located in the dotted frame in (d) indicate the Moiré patterns frequently observed in TEM images.

bubbles with an ultrathin wall, although some nanoparticles with a diameter of tens of nanometers can be occasionally observed (marked by black dotted cycles in Figure 2b; Supporting Information, Figure S3). The thickness of the ultrathin wall of these bubbles can be analyzed statistically from the high-resolution TEM (HRTEM) images, which is 6.41 Å on average and close to cubic lattice constant of CeO_2 (5.4113 Å) (Figure 2c,d). It should be noted that any organic ligands or capping agents, which are generally involved in wet chemistry processes to stabilize the crystalline nanostructures, can be safely excluded in this ceria foam because only one multiple metal oxide $CeGeO_4$ crystals were used as solid precursor and the temperature applied was relatively high (ca. 780 °C) during the formation of ceria foam.[17,18] Furthermore, HRTEM results provide additional evidence for the crystallinity and growth characteristics of these ultrathin walls; most of these walls grow along the [111] direction. Figure 2d shows the wall with a lattice fringe of 0.32 nm corresponding to the (111) lattice spacing of cubic ceria crystal, and the corresponding fast Fourier transform (FFT) pattern exhibits an array of spots that can be indexed as the {111} facets. White arrows in Figure 2d indicate the edges of the ultrathin walls, and the lattice fringe can be identified continuously across the entire surface. All of the structural evidences analyzed indicate that the wall of CeO_2 foam has a thickness on atomic scale, while single-crystalline characteristics are maintained. The curved surface of CeO_2 foam might be attributed to the different bonding energies and states of Ce^{3+} and Ce^{4+} in the ultrathin single-crystalline wall of CeO_2 (Supporting Information, Figure S4). The real shape of the CeO_2 foam can be thus imitated by common soap bubbles (Figure 2e).

To identify the bonding states of elements Ce, Ge, and O, X-ray photoelectron spectroscopy (XPS) was used to probe the component and valance state of the CeO_2 foam (Supporting Information, Figure S4). The O 1s XPS spectrum can be deconvoluted into three major states, which are located at 529.5, 530.8, and 531.7 eV. Praline et al. reported that oxygen coordinated to Ce^{4+} showed a lower binding energy than oxygen bound to Ce^{3+} in CeO_2.[19] Thus, peaks located at 529.5 and 530.8 eV can be safely assigned to oxygen bound to Ce^{4+} and Ce^{3+}, respectively, and the relative ratio of Ce^{3+} is 20.7%. Moreover, peak located at 531.7 eV can be assigned to oxygen bound to residual Ge^{4+}, which is consistent with previous report.[20] Combined the XPS results with XRD evidence shown in Figure 1, it can be confirmed that residual elemental Ge should be present as amorphous GeO_x. The nitrogen adsorption–desorption isotherms and the Barrett–Joyner–Halenda (BJH) pore size distributions calculated from the adsorption branch indicate that the CeO_2 foams have a BET surface area of 60.1 $m^2 g^{-1}$ and a pore volume of 0.19 $cm^3 g^{-1}$ (Figure 3). The relative low surface area of ceria foam might be due to the lack of aperture on the atomically thin walls.

To elucidate the chemistry reported above, systematic first-principles calculations were performed. The HRTEM image of the well-defined $CeGeO_4$ crystals indicates that the external surfaces consist mainly of {101} facets (Supporting Information, Figure S5). The (101) surface could exhibit two types of terminations, and an A-type termination configuration (both Ce^{4+} and Ge^{4+} exposed) was employed in the

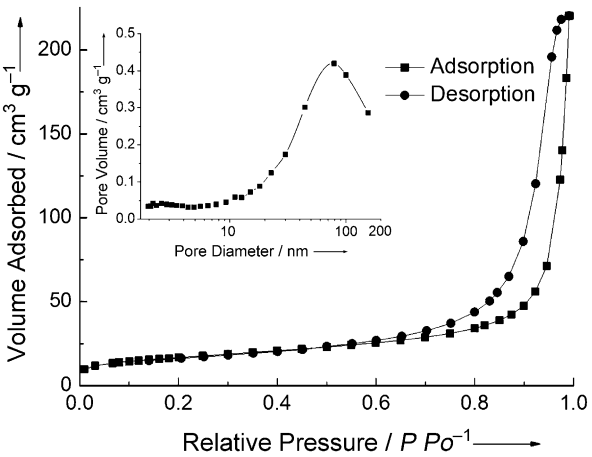

Figure 3. The nitrogen adsorption–desorption isotherms of CeO_2 foam and BJH pore-size distributions (inset) from adsorption branches.

modeling owing to its lower surface energy than that of B-type (only Ce^{4+} exposed). For the A-type (101) surface, a $(2 \times \sqrt{5}/2)$ R23° surface supercell containing 48 atoms with a slab vacuum distance of 15 Å in the (101) direction was formed and the optimized structure is shown in Figure 4a,b. On the surface, possible elementary reactions relating to NH_3 dehydrogenation and oxidation were calculated, aiming at shedding light on the origin of NH_3-induced $CeGeO_4$ crystal decomposition at high temperature.

As shown in Figure 4a,b, there are five kinds of O atoms on $CeGeO_4$ (101). It was found from our calculations that O_I bonded to two Ce^{4+} and O_{II} bonded to Ce^{4+} and Ge^{4+} exhibit higher reactivities than other O atoms, and thus these two kinds of oxygen were considered for the reactions. NH_3 can adsorb on the Ge^{4+} or Ce^{4+} with almost identical chemisorption energy (1.14 eV). The adsorbed NH_3 at the Ge^{4+} site can dissociate into NH_2 species, releasing a H to the nearest O_I by overcoming a barrier as low as 0.18 eV. However, NH_3 adsorbed at the Ce^{4+} site can hardly dehydrogenate (simple geometric optimization of dissociated configuration would recover the initial NH_3 adsorption state) and thus the subsequent reactions at the Ce^{4+} site were not considered. Moreover, OH_I can transfer its H to the nearest O_{II} easily by overcoming a barrier of 0.34 eV, and then the recovered O_I continues to abstract H from NH_2 with a low barrier of 0.28 eV. Similarly, by virtue of O_I, NH can finally dissociate into atomic N with a barrier as low as 0.07 eV. The surface N atom (N*) can further react with O_I to form NO readily by surmounting a low barrier of 0.08 eV, and NO can desorb easily owing to its low chemisorption energy (0.30 eV) at the Ge^{4+} site. Interestingly, we found that gaseous NO may re-adsorb at the O_I or O_{II} site to form an [ONO] complex with a chemisorption energy of 1.37 eV and 1.01 eV, respectively, and this complex can be released to form NO_2. XPS spectroscopy also detected NO_3^- on the surface of CeO_2 foam, which is the evidence of NO_2 formation (Supporting Information, Figure S4a). As the reaction proceeds, the surface OH_I or OH_{II} can react with each other or by receiving a diffusing H to form H_2O*, which can easily desorb from the surface at high temperature at an energy cost of 0.58 eV and

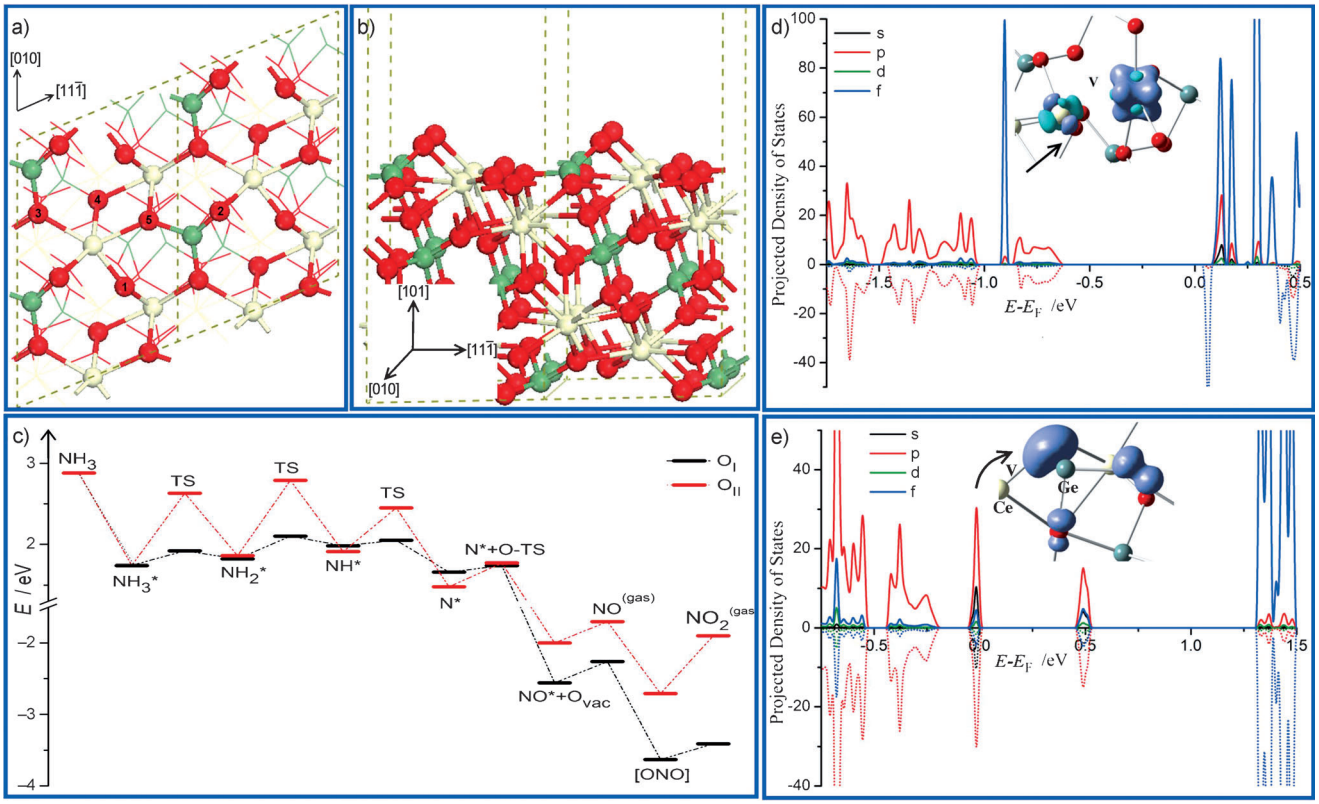

Figure 4. a,b) Top and side view of $CeGeO_4$ (101) surface. O red, Ge green, Ce white. c) Energy profiles of the NH_3 oxidation progress involving O_I and O_{II}. d,e) Projected DOS of the reduced (101) surface with a d) O_I or e) O_{II} vacancy. Insets: 3d isosurfaces of the dominating gap state near the top of valence band.

0.90 eV, respectively. When surface O_I are removed, NH_3 will attack O_{II} in a way similar with O_I described above. From the energy profile obtained on the O_{II} site (Figure 4c), it can be seen that, relative to the adsorbed NH_3, the highest point in the energy profile is 1.05 eV. Thus under the experimental conditions herein ($T \approx 1053$ K), the removal of O_{II} by an NH_3 molecule is expected to occur without any difficulty. The whole reaction mechanism can be summarized as folows:

$$\text{dehydrogenation}: NH_3{}^* + 3\,O \rightarrow N^* + 3\,OH, \quad OH + OH \rightarrow H_2O + O_{vac} \tag{1}$$

$$\text{oxidation}: N^* + O \rightarrow NO_x + {}^* + O_{vac} \tag{2}$$

where * denotes an uncovered Ge^{4+} or Ce^{4+} site. O can be O_I or O_{II}, and O_{vac} represents the corresponding oxygen vacancy. The produced gaseous NO_x and H_2O could contribute to the formation of the foam-like structure during the process. As the reaction proceeds, NH_3 would gradually erode into the body of the $CeGeO_4$ crystal and reforms into NO_x and H_2O, whch may cause high internal pressure at high temperature, which serves as one of the key dynamic forces for recrystallizing in an expansion mode.

With the first-principles calculations above, it is clear that NH_3 can remove the surface-exposed O_I and O_{II}, which eventually lead to the surface reduction. The electronic structure of the system in the presence of an O_I or O_{II} vacancy was also analyzed. Figure 4d shows the projected density of states of $CeGeO_4$ (101) with an O_I vacancy, which shows that at the top of valence band, a very sharp f-gap state and a minor p-band peak can be observed. Integrating this f-gap state gives 1.64 e. In conjunction with the isosurface plot of charge density of this gap state (insert in Figure 4d), it can be seen that the two excess electrons mainly localize in the 4f orbital of the two nearest Ce^{4+} and reduce them to Ce^{3+}, in agreement with the XPS result regarding the detection of a number of Ce^{3+} on the material surface after NH_3 treatment (Supporting Information, Figure S4). Together with the local density of state analysis, the presence of minor p-gap state indicates that O_I removal induces a slight reduction of the second-nearest neighbor Ge^{4+}. Similar analyses show that the two excess electrons primarily localize in the 4p and 4s orbital of the nearest Ge^{4+} when O_{II} is removed (Figure 4e). Integrating the 4p gap state gives a 1.57 e and Bader charge shows that Ge^{4+} gains 1.85 e as O_{II} is removed, indicating the formation of Ge^{2+}. Herein, two interesting points are worth noting: 1) There is a small number of electrons transferred to the 2p orbital of three O linking with the reduced Ge^{4+} owing to the enhancement of these Ge–O bonds by compensating for the missing Ge-O_{II}, as shown in the 3d isosurface plot in Figure 4e; and 2) compared with the well-known facile reduction of Ce^{4+} into Ce^{3+}, on removing O_{II} which bonds with a Ce^{4+} and a Ge^{4+}, the reduction of Ge^{4+} into Ge^{2+} ions takes place preferentially. In the case that a number of Ge^{2+} are formed on the surface, they may be gasified as GeO when the temperature achieves the boiling point of GeO (710 °C),

which is consistent with the weight decrease of the samples after heat treatment under NH_3 atmosphere. The GeO vapor might further react with NH_3 to form germanium nitride.[21,22] The removal of GeO may further destroy the crystal structure and eventually lead to the decomposition of the $CeGeO_4$ and the formation of CeO_2 foam.

In summary, CeO_2 foam with ultrathin single-crystalline walls was synthesized successfully by thermally decomposing $CeGeO_4$ crystals at NH_3 atmosphere. The feasibility and reaction pathways of nitridation process were analyzed using the first-principles calculations, which indicates that O element on the {101} facets of orthogermanate $CeGeO_4$ can be removed by NH_3 as a result of forming Ce^{3+} and Ge^{2+}. The Ge^{2+} may be gasified as GeO at high temperature, which leads to the decomposition of the $CeGeO_4$ crystals and formation of CeO_2 foam. The results in this work provide a facile approach to construct porous foam of ceria with atomically thin single-crystalline walls, as well as open the door for other technologically important applications.

Received: December 10, 2011
Revised: January 14, 2012
Published online: February 28, 2012

Keywords: CeO_2 · density function theory · foams · single crystals

[1] J. H. Pan, H. Dou, Z. Xiong, C. Xu, J. Ma, X. S. Zhao, *J. Mater. Chem.* **2010**, *20*, 4512 – 4528.
[2] M. C. Orilall, U. Wiesner, *Chem. Soc. Rev.* **2011**, *40*, 520 – 535.
[3] C. Y. Ma, Z. Mu, J. J. Li, Y. G. Jin, J. Cheng, G. Q. Lu, Z. P. Hao, S. Z. Qiao, *J. Am. Chem. Soc.* **2010**, *132*, 2608 – 2613.
[4] K. Cheng, S. Sun, *Nano Today* **2010**, *5*, 183 – 196.
[5] S. Zhang, L. Chen, S. Zhou, D. Zhao, L. Wu, *Chem. Mater.* **2010**, *22*, 3433 – 3440.
[6] F. Zhang, D. Gu, T. Yu, F. Zhang, S. Xie, L. Zhang, Y. Deng, Y. Wan, B. Tu, D. Zhao, *J. Am. Chem. Soc.* **2007**, *129*, 7746 – 7747.
[7] Y. Shi, Y. Wan, R. Liu, B. Tu, D. Zhao, *J. Am. Chem. Soc.* **2007**, *129*, 9522 – 9531.
[8] P. Yang, D. Zhao, D. I. Margolese, B. F. Chmelka, G. D. Stucky, *Chem. Mater.* **1999**, *11*, 2813 – 2826.
[9] U. Ciesla, S. Schacht, G. D. Stucky, K. K. Unger, F. Schüth, *Angew. Chem.* **1996**, *108*, 597 – 600; *Angew. Chem. Int. Ed. Engl.* **1996**, *35*, 541 – 543.
[10] Q. Fu, H. Saltsburg, M. Flytzani-Stephanopoulos, *Science* **2003**, *301*, 935 – 938.
[11] A. Trovarelli, *Catal. Rev. Sci. Eng.* **1996**, *38*, 439 – 520.
[12] E. P. Murray, T. Tsai, S. A. Barnett, *Nature* **1999**, *400*, 649 – 651.
[13] A. Corma, P. Atienzar, H. Garcia, J. Y. Chane-Ching, *Nat. Mater.* **2004**, *3*, 394 – 397.
[14] L. Tye, N. A. El-Masry, T. Chikyowm, P. McLarty, S. M. Bedair, *Appl. Phys. Lett.* **1994**, *65*, 3081 – 3083.
[15] A. H. Morshed, M. E. Moussa, S. M. Bedair, R. Leonard, S. X. Liu, N. ElMasry, *Appl. Phys. Lett.* **1997**, *70*, 1647 – 1649.
[16] W. C. Chueh, C. Falter, M. Abbott, D. Scipio, P. Furler, S. M. Haile, A. Steinfeld, *Science* **2010**, *330*, 1797 – 1801.
[17] C. Liu, H. Sun, S. Yang, *Chem. Eur. J.* **2010**, *16*, 4381 – 4393.
[18] T. Yu, B. Lim, Y. Xia, *Angew. Chem.* **2010**, *122*, 4586 – 4589; *Angew. Chem. Int. Ed.* **2010**, *49*, 4484 – 4487.
[19] G. Praline, B. E. Koel, R. L. Hance, H. I. Lee, J. M. White, *J. Electron Spectrosc. Relat. Phenom.* **1980**, *21*, 17 – 30.
[20] K. Kato, H. Kondo, M. Sakashita, S. Zaima, *Thin Solid Films* **2010**, *518*, S226 – S230.
[21] K. Maeda, N. Saito, Y. Inoue, K. Domen, *Chem. Mater.* **2007**, *19*, 4092 – 4097.
[22] S. Shimada, Y. Miura, A. Miura, *Cryst. Growth Des.* **2007**, *7*, 1251 – 1255.

